

# Feasibility of simultaneous EEG-fMRI at 0.55 T: Recording, Denoising, and Functional Mapping

Parsa Razmara, Takfarinas Medani, Majid Abbasi Sisara, Anand A. Joshi, Rui Chen, Woojae Jeong, Ye Tian, Krishna S. Nayak, and Richard M. Leahy

University of Southern California, Los Angeles, CA, USA

**Abstract**—Simultaneous recording of electroencephalography (EEG) and functional MRI (fMRI) can provide a more complete view of brain function by merging high temporal and spatial resolutions. High-field ( $\geq 3$ T) systems are standard, and require technical trade-offs, including artifacts in the EEG signal, reduced compatibility with metallic implants, high acoustic noise, and artifacts around high-susceptibility areas such as the optic nerve and nasal sinus. This proof-of-concept study demonstrates the feasibility of simultaneous EEG-fMRI at 0.55T in a visual task. We characterize the gradient and ballistocardiogram (BCG) artifacts inherent to this environment and demonstrate that the lower field strength reduces the magnitude of the BCG artifact compared to conventional 3T systems. This reduction shows promise for facilitating effective denoising while preserving the alpha rhythm and signal integrity. Furthermore, we tested a multimodal integration pipeline and demonstrated that the EEG power envelope corresponds with the hemodynamic BOLD response, supporting the potential to measure neurovascular coupling in this environment. We demonstrate that combined EEG-fMRI at 0.55T is feasible and represents a promising environment for multimodal neuroimaging.

**Index Terms**—Mid-Field MRI, EEG-fMRI, Multimodal Neuroimaging, Artifact Removal, BOLD.

## I. INTRODUCTION

Simultaneous electroencephalography (EEG) and functional MRI (fMRI) recording is a valuable multimodal approach that provides complementary insights into brain function, with EEG offering high temporal resolution and fMRI providing spatial detail [1], [2]. fMRI has traditionally relied on higher-field MRI systems ( $\geq 3$ T) to maximize the blood oxygenation level-dependent (BOLD) sensitivity, resolution, and spatial specificity inherent to stronger magnetic fields [3]–[6]. This creates a challenging environment for multimodal integration. Higher-field MRI introduces substantial trade-offs, including magnetic field-induced artifacts in the EEG signal, increased sensitivity to  $B_0$  field inhomogeneities, and reduced compatibility for subjects with implants such as neurostimulators [7]–[9].

The recent resurgence of lower-field systems ( $\leq 1$ T) for general MRI applications [7], [10]–[15], driven by modern 0.55T systems equipped with high-performance gradients, offers a compelling solution to these limitations [7], [15]. Unlike historical lower-field scanners that were constrained by limited gradient performance, contemporary 0.55T systems

The authors receive grant support from the National Institutes of Health (R01EB026299, U01EB023820) and the National Science Foundation (No. 1828736).

support functional imaging using advanced gradient hardware. However, imaging at 0.55T operates with reduced intrinsic SNR, where signal estimation can benefit from statistical modeling and regularization principles in MRI analysis [16], [17]. The primary benefit lies in the reduced interaction between the static magnetic field and the EEG recording equipment. Lower field strength is expected to significantly attenuate the ballistocardiogram (BCG) artifact, a persistent noise source linked to cardiac motion in the magnetic field, while simultaneously improving compatibility with patients who use neurostimulators or other implanted devices [7], [8]. This distinct combination of high-performance imaging and reduced electromagnetic interference positions the 0.55T system as a favorable platform for expanding neuroimaging to populations currently excluded from higher-field studies.

Recent studies have also demonstrated the feasibility of fMRI at 0.55T [18]–[20]. Nonetheless, integrating EEG with 0.55T MRI presents specific technical challenges, primarily due to gradient-induced artifacts (GA) and ballistocardiogram (BCG) interference [8], [21]. These artifacts, while present in all MRI settings, can present unique characteristics at 0.55T systems, necessitating tailored approaches to ensure reliable EEG signal quality.

This pilot study investigates the feasibility of simultaneous EEG-fMRI recording within a 0.55T MRI environment, aiming to understand the impact of this environment on EEG data quality and to assess preliminary methods for reducing artifact interference. To our knowledge, this is the first study that has explored EEG recording within a 0.55T MRI. This study seeks to validate the potential of such a setup for neuroimaging applications and to develop foundational techniques that could enable future multimodal studies in diverse clinical and research environments. To compensate for the reduced intrinsic BOLD sensitivity of the 0.55T MRI signal, we utilized extended acquisition durations (10-minute concatenated runs). Our preliminary work at 0.55T [19] has demonstrated that such extended durations drive substantial gains in sensitivity, yielding activation strengths comparable to standard higher-field acquisitions [2], [22], thereby providing a functional context for investigating the benefits of the cleaner electromagnetic environment for EEG recording. Furthermore, we tested a multimodal integration pipeline and demonstrated that the EEG power envelope corresponds with the hemodynamic BOLD response, supporting the potential to measure neurovascular coupling in this environment. We demonstrate

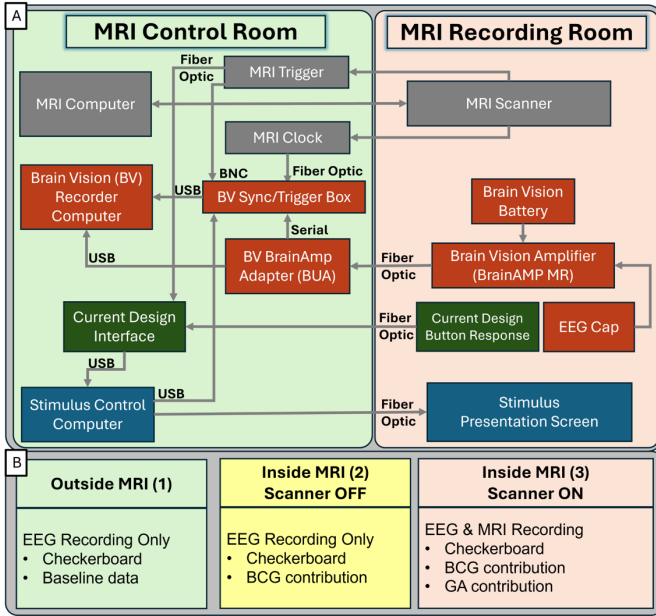


Fig. 1. (A) Schematic of the simultaneous EEG-fMRI setup showing synchronization between the MRI trigger and the BrainVision recorder. (B) Protocol overview for Outside, Scanner OFF, and Scanner ON conditions.

that combined EEG-fMRI at 0.55T is feasible and represents a promising environment for multimodal neuroimaging.

## II. METHODS

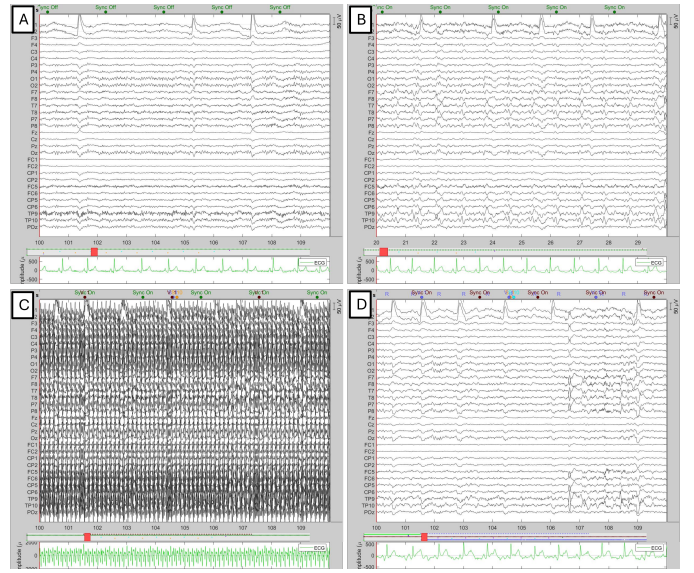
### A. Experimental Methods

Two healthy adult subjects were enrolled under a protocol approved by our Institutional Review Board, after providing written informed consent. Data collection was performed under three distinct conditions to isolate artifact sources: 1) **Outside MRI**, where baseline EEG was recorded to capture true neural activity without scanner-induced interference; 2) **Inside MRI (Scanner OFF)**, capturing the contribution of the BCG—induced by cardiac motion within the static magnetic field—without GA interference; and 3) **Inside MRI (Scanner ON)**, involving fully simultaneous EEG-fMRI recording to capture the integrated effect of BCG and GA.

Tasks included a flickering checkerboard (visual stimulation) following an established block design. The visual task involved 24-second blocks alternating with rest [2], [19]. The experimental setup and protocol timing are illustrated in Fig. 1.

### B. Hardware and Data Acquisition

Imaging was conducted on a 0.55T scanner (prototype MAGNETOM Aera, Siemens Healthineers, Forchheim, Germany) equipped with high-performance gradients (45 mT/m amplitude, 150 T/m/s slew rate) [7], [23] and a 16-channel head-neck receive array. Functional data were acquired using a single-shot EPI BOLD sequence (FOV:  $210 \times 170$  mm $^2$ , voxel size:  $3.3 \times 3.3 \times 4$  mm $^3$ , TR: 3000 ms, TE: 85 ms), with twenty interleaved axial slices to achieve whole-cerebrum



coverage [19]. Simultaneous EEG was recorded using a 32-channel MR-compatible BrainCap and BrainAmp MR system (Brain Products GmbH, Gilching, Germany). To minimize GA jitter, the EEG system was phase-locked to the MRI clock via a sync-trigger box. GA correction and BCG removal were performed as described in Fig. 2.

### C. Processing Pipelines

The fMRI data were utilized using the BrainSuite fMRI Pipeline (BFP) and SPM12 [16], [24], [25]. Preprocessing included slice-timing correction, motion correction, 8mm FWHM spatial smoothing, and 0.005 Hz high-pass filtering [16]. To achieve robust statistical power, two 5-minute runs were concatenated to form a 10-minute dataset for the final analysis [19].

The EEG denoising pipeline utilized the BrainVision Analyzer [26] and Brainstorm [27] to address the specific noise profile of the 0.55T scanner. GA correction was performed using Average Artifact Subtraction (AAS) [21]. BCG artifacts were removed using a pulse-artifact subtraction method based on the concurrent ECG channel. Finally, Independent Component Analysis (ICA) was applied to isolate residual artifacts from neural components followed by visual inspection of the final data, where a few channels were marked as bad and excluded from the analysis.

### D. Multimodal Data Integration

To evaluate the coupling between electrophysiological activity and the hemodynamic response, we performed a voxel-wise correlation analysis comparing the observed BOLD fMRI signal with two distinct predictive models: a data-driven EEG predictor and a hypothesis-driven block-design model.

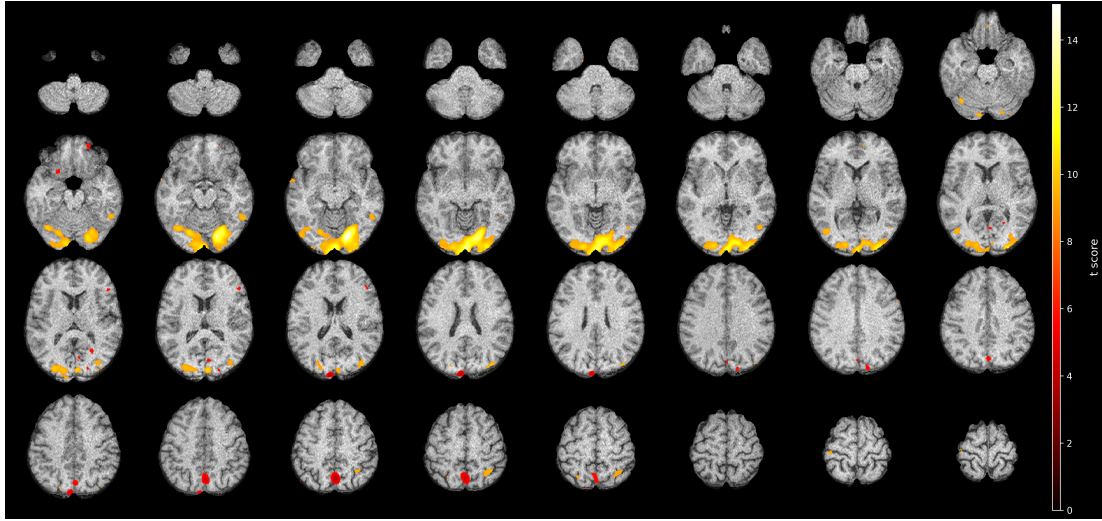


Fig. 3. Visual activation and statistical reliability at 0.55T. Representative whole-brain axial montage of t-statistic maps from a single participant, generated from 10 minutes of concatenated task data. Activation maps are overlaid on the 0.55T T1-weighted anatomical image. Significant, contiguous clusters are localized to the primary visual cortex (V1) and surrounding occipital regions. Statistical maps are thresholded at  $q < 0.05$  (FDR-corrected) to demonstrate the spatial extent and reliability of the BOLD signal at 0.55T.

1) *Construction of the EEG-Informed Predictor:* The expected BOLD time course was derived directly from the subject's neural data by isolating the Steady-State Visual Evoked Potential (SSVEP) [2], [15] from the Oz electrode, which is maximally sensitive to visual stimulation. The preprocessing pipeline comprised three steps: 1) **spectral isolation**, where the preprocessed Oz time series was bandpass filtered between 11 Hz and 13 Hz (20th-order IIR filter) to isolate the target checkerboard frequency; 2) **power extraction**, in which the instantaneous amplitude envelope was computed using the Hilbert transform to quantify neural power fluctuations over time; and 3) **hemodynamic modeling**, where this power envelope was downsampled to the fMRI repetition time (TR = 3.0 s) and convolved with a canonical Hemodynamic Response Function (SPM-HRF) to account for neurovascular delay.

2) *Statistical Mapping:* We calculated the Pearson correlation coefficient ( $r$ ) between the measured fMRI time series at each voxel and two predictors: (1) the standard Block Design boxcar model, and (2) the EEG-derived power envelope. This generated two independent spatial maps representing voxels synchronized with the experimental timing and voxels synchronized with the subject's actual neural power at 12 Hz.

### III. RESULTS

#### A. Significant Visual Activation at 0.55T

Significant activation ( $p < 0.05$ , FDR corrected) was consistently observed in the visual cortex across participants, as shown in the statistical maps in Fig. 3. Utilizing the 10-minute concatenated protocol, activation was localized to the primary visual cortex (V1) and adjacent visual areas. The analysis yielded a mean t-score of 9.0, demonstrating that detection of task-based BOLD signal changes is feasible at 0.55T with extended scanning durations [19].

#### B. EEG Signal Quality and Artifact Characterization

Analysis of the 0.55T environment reveals a distinct and favorable artifact profile. We observed that the magnitude of the BCG artifact was reduced compared to typical reports from high-field (3T) systems, consistent with the physics of lower magnetic field strengths. This reduction facilitated effective denoising using standard gradient and BCG subtraction techniques without the need for aggressive filtering that might compromise neural data. Power Spectral Density (PSD) analysis (Fig. 4) confirms the preservation of the physiological alpha rhythm (8-13 Hz) in the cleaned data.

Furthermore, the topographical distribution of the SSVEP power modulation (Fig. 5) indicates focal activation over occipital electrodes, demonstrating that spatial information is preserved after artifact removal.

#### C. Spatial Correspondence of Activation Maps

The multimodal correlation analysis showed a similar spatial pattern between the data-driven EEG predictor and the standard block design in the occipital lobe. As shown in Fig. 6, the EEG-informed model (Fig. 6A), based on the  $O_z$  power envelope, identified significant activation clusters localized to the primary visual cortex (V1) and surrounding visual areas. This spatial map is similar to the standard block-design activation (Fig. 6B), suggesting that the recovered EEG signal captures the expected physiological changes in the visual cortex. These results provide initial evidence that at 0.55 T, the 12 Hz rhythmic power can be used to track the BOLD response, supporting the feasibility of using simultaneous EEG-fMRI for functional mapping at this field strength.

### IV. DISCUSSION AND CONCLUSION

This pilot study suggests that simultaneous EEG-fMRI is feasible and promising at 0.55T. By employing a 10-minute

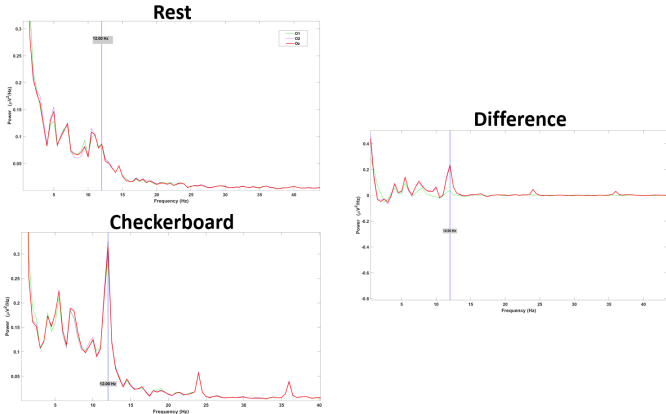


Fig. 4. Spectral characterization and task-evoked oscillatory responses at 0.55 T. Power Spectral Density (PSD) analysis across recording conditions (Rest vs. Checkerboard) for occipital channels ( $O_z$ ,  $O_1$ , and  $O_2$ ) demonstrates the fidelity of neural signal recovery. The spontaneous alpha rhythm (8–13 Hz) is preserved in the resting-state data following artifact subtraction, serving as a baseline indicator of signal integrity. During the visual task, the power spectrum exhibits a robust fundamental response at the 12 Hz stimulation frequency, with distinctly identifiable higher-order harmonics at 24 Hz and 36 Hz. The spectral difference plot (right) highlights the narrow-band power localized to these frequencies, confirming that the denoising pipeline effectively suppresses scanner-induced interference while retaining both physiological and task-specific spectral features.

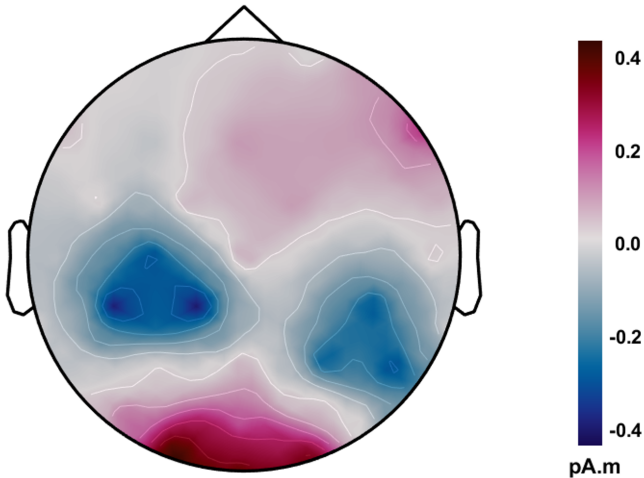


Fig. 5. Topographical distribution of SSVEP power modulation at 0.55 T. The heatmap illustrates the spatial distribution of the spectral power difference (Checkerboard – Rest) at the 12 Hz stimulation frequency. A highly focal activation is centered over the occipital electrodes ( $O_z$ ,  $O_1$ , and  $O_2$ ), consistent with the primary generators of the visual evoked response. This localized topography confirms that the signal recovery pipeline suppressed widespread scanner-induced artifacts while preserving the underlying spatial integrity of the neural data in the mid-field environment.

concatenated acquisition protocol, we observed significant BOLD activation in the visual cortex, comparable to patterns typically reported in conventional-field studies, despite the inherent SNR challenges of 0.55T [19]. These findings support the utility of high-performance 0.55T systems for functional neuroimaging when acquisition protocols are tailored to the specific characteristics of the lower-field environment.

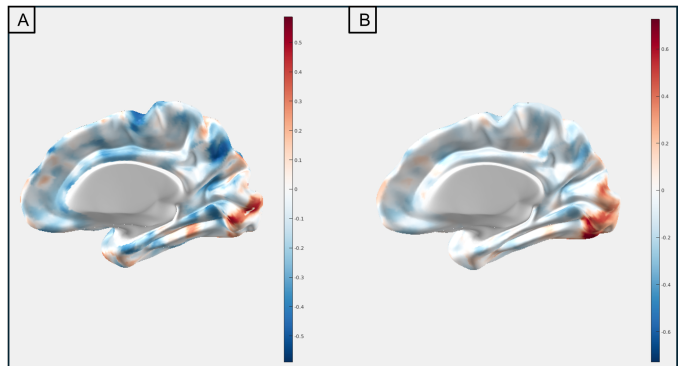


Fig. 6. Multimodal functional mapping and neurovascular coupling at 0.55 T. Representative cortical correlation maps from a 5-minute run in a single participant demonstrate the spatial distribution of Pearson correlation coefficients ( $r$ ). (A) Functional map derived from the voxel-wise correlation between the measured BOLD signal and the data-driven 12 Hz power envelope extracted from the  $O_z$  electrode. (B) Functional map derived using the hypothesis-driven block design (Boxcar convolved with a canonical HRF). The high degree of spatial correspondence between the EEG-informed predictor and the standard model validates the integrity of the multimodal integration and confirms that the BOLD signal at 0.55 T remains tightly coupled to underlying electrophysiological power modulation.

A notable advantage observed in this environment is the favorable artifact profile for EEG. The magnitude of the BCG artifact appeared reduced compared to higher-field magnets, consistent with the physics of magnetic field interactions. This reduction likely contributed to the efficacy of standard denoising pipelines, allowing for the preservation of physiological signals such as the alpha rhythm and SSVEP without the need for aggressive filtering that might compromise data integrity.

The multimodal analysis provides preliminary evidence for neurovascular coupling at 0.55T. The spatial correspondence between the activation maps derived from the standard block design and the data-driven EEG regressor (Fig. 6) indicates that the BOLD signal in the visual cortex is tightly coupled to the underlying electrophysiological power in the 12 Hz band. This result serves as a technical validation of the multimodal acquisition pipeline, suggesting that the EEG signal can serve as a viable predictor of hemodynamic activity in this environment.

These results, while drawn from a pilot cohort ( $N = 2$ ), establish a proof-of-concept for multimodal imaging at 0.55T. The demonstration of significant BOLD activation, high-fidelity recovery of focal SSVEP signatures, and the observed spatial correspondence between electrophysiological and hemodynamic signals support the technical viability of this mid-field platform. Contemporary mid-field systems offer practical advantages in accessibility and device compatibility that may broaden neuroimaging applications where higher-field scanners are unsuitable [15]. Neurovascular coupling underlies the BOLD signal [28], [29], and multimodal EEG-fMRI frameworks are increasingly investigated for objective characterization of neurological disorders [1], [30]. The reduced artifact burden observed at 0.55T may provide a technically favorable environment for future multimodal

investigations of variations in neurovascular dynamics.

#### ACKNOWLEDGMENT

We thank Sophia X. Cui (Siemens Healthineers) for technical support, and Mary Yung for research coordination.

#### REFERENCES

- [1] T. Warbrick, "Simultaneous EEG-fMRI: What Have We Learned and What Does the Future Hold?" *Sensors*, vol. 22, no. 6, p. 2262, 2022.
- [2] Q. K. Telesford, et al., "An open-access dataset of naturalistic viewing using simultaneous EEG-fMRI," *Sci. Data*, vol. 10, no. 1, p. 554, 2023.
- [3] K. R. Thulborn, "Clinical rationale for very-high-field (3.0 Tesla) functional magnetic resonance imaging," *Top. Magn. Reson. Imaging*, vol. 10, no. 1, pp. 37–50, 1999.
- [4] J. H. Duyn, "The future of ultra-high field MRI and fMRI for study of the human brain," *Neuroimage*, vol. 62, no. 2, pp. 1241–1248, 2012.
- [5] K. Ugurbil, "Imaging at ultrahigh magnetic fields: History, challenges, and solutions," *Neuroimage*, vol. 168, pp. 7–32, 2018.
- [6] F. De Martino, et al., "The impact of ultra-high field MRI on cognitive and computational neuroimaging," *Neuroimage*, vol. 168, pp. 366–382, 2018.
- [7] A. E. Campbell-Washburn, et al., "Opportunities in interventional and diagnostic imaging by using high-performance low-field-strength MRI," *Radiology*, vol. 293, no. 2, pp. 384–393, 2019.
- [8] G. Srivastava, et al., "ICA-based procedures for removing ballistocardiogram artifacts from EEG data acquired in the MRI scanner," *Neuroimage*, vol. 24, no. 1, pp. 50–60, 2005.
- [9] B. P. Sutton and F. Lam, "Imaging in the presence of magnetic field inhomogeneities," *Magnetic Resonance Image Reconstruction*, Academic Press, pp. 327–354, 2022.
- [10] M. Sarracanie, et al., "Low-cost high-performance MRI," *Sci. Rep.*, vol. 5, p. 15177, 2015.
- [11] J. P. Marques, et al., "Low-field MRI: An MR physics perspective," *J. Magn. Reson. Imaging*, vol. 49, no. 6, pp. 1528–1542, 2019.
- [12] L. L. Wald, et al., "Low-cost and portable MRI," *J. Magn. Reson. Imaging*, vol. 52, no. 3, pp. 686–696, 2020.
- [13] J. P. Marques, et al., "When less is more: the view of MRI vendors on low-field MRI," *MAGMA*, vol. 34, no. 4, pp. 479–482, 2021.
- [14] A. Halder, et al., "Optimization of Gradient-Echo Echo-Planar Imaging for T2\* Contrast in the Brain at 0.5 T," *Sensors*, vol. 23, no. 20, p. 8428, Oct. 2023.
- [15] T. C. Arnold, et al., "Low-field MRI: Clinical promise and challenges," *J. Magn. Reson. Imaging*, vol. 57, no. 1, pp. 25–44, 2023.
- [16] K. J. Friston, et al., "Statistical parametric maps in functional imaging: a general linear approach," *Human Brain Mapping*, vol. 2, no. 4, pp. 189–210, 1994.
- [17] P. Razmara, et al., "Advancements in Prostate Luminal Water Imaging: Radial Turbo Spin-Echo Acquisition and Spatial Regularization," *Proc. Intl. Soc. Magn. Reson. Med.*, 2024.
- [18] Y. Wang, et al., "fMRI based on transition-band balanced SSFP in comparison with EPI on a high-performance 0.55 T scanner," *Magn. Reson. Med.*, vol. 85, no. 6, pp. 3196–3210, 2021.
- [19] P. Razmara, et al., "A feasibility study of task-based fMRI at 0.55 T," *Proc. Intl. Soc. Mag. Reson. Med.*, vol. 33, p. 0491, 2025.
- [20] P. A. Bandettini, "Twenty years of functional MRI: The science and the stories," *Neuroimage*, vol. 62, no. 2, pp. 575–588, 2012.
- [21] P. J. Allen, et al., "A method for removing imaging artifact from continuous EEG recorded during functional MRI," *Neuroimage*, vol. 12, no. 2, pp. 230–239, 2000.
- [22] R. B. Tootell, et al., "Functional analysis of human MT and related visual cortical areas using magnetic resonance imaging," *J. Neurosci.*, vol. 15, no. 4, pp. 3215–3230, 1995.
- [23] Y. Tian, et al., "New clinical opportunities of low-field MRI: heart, lung, body, and musculoskeletal," *MAGMA*, vol. 37, no. 1, pp. 1–14, 2024.
- [24] A. A. Joshi, et al., "BFP: BrainSuite fMRI pipeline," *OHBM*, 2018.
- [25] D. W. Shattuck and R. M. Leahy, "BrainSuite: an automated cortical surface identification tool," *Med. Image Anal.*, vol. 6, no. 2, pp. 129–142, 2002.
- [26] BrainVision Analyzer (Version 2.2.0) [Software], Brain Products GmbH, Gilching, Germany, 2019.
- [27] F. Tadel, et al., "Brainstorm: A user-friendly application for MEG/EEG analysis," *Comput. Intell. Neurosci.*, 2011.
- [28] C. Iadecola, "Neurovascular regulation in the normal brain and in Alzheimer's disease," *Nature Reviews Neuroscience*, vol. 5, no. 5, pp. 347–360, 2004.
- [29] H. Girouard and C. Iadecola, "Neurovascular coupling in the normal brain and in hypertension, stroke, and Alzheimer disease," *Journal of Applied Physiology*, vol. 100, no. 1, pp. 328–335, 2006.
- [30] M. A. Ranjbar, A. Ghaleh, H. B. Dogaheh, P. Razmara, and M. Baghani, "Beyond subjective measures: Systematic review of deep learning in chronic pain: Modalities, methods, and applications," <https://doi.org/10.21203/rs.3.rs-6217737/v1>, 2025.